Petroleum Science 23 (2026) 4545–4558

Contents lists available at ScienceDirect

Petroleum Science

journal homepage: www.keaipublishing.com/en/journals/petroleum-science

Original Paper

Quantifying the through-going evolution of strike-slip fault zones: Insights from analogue modeling

Guang-Hui Wu[a,b,*], Chen Qiu[a], Hao Tang[a], Zhou Xie[c], Xin Chen[a], Heng-You Li[a], Zhe-Yu Luo[a], Chong Sun[c]

[a] School of Geoscience and Technology, Southwest Petroleum University, Chengdu, 610500, Sichuan, China
[b] State Key Laboratory of Oil and Gas Reservoir Geology and Exploitation, Southwest Petroleum University, Chengdu, 610500, Sichuan, China
[c] PetroChina Tarim Oilfield Company, Korla, 841000, Xinjiang, China

ARTICLE INFO

Article history:
Received 4 January 2024
Received in revised form
12 January 2026
Accepted 29 May 2026
Available online 3 June 2026

Edited by Xiu-Fang Hu

Keywords:
Strike-slip fault
Fault segmentation
Through-going evolution
Quantitative analogue modeling
Fault growth
Intracratonic basin

ABSTRACT

Large strike-slip fault zones commonly develop through-going architectures through progressive linkage of fault segments. However, quantitatively characterizing the through-going evolution of strike-slip fault zones remains challenging. Based on the pure strike-slip tectonic setting of the Tarim Basin, twelve sandbox analogue experiments were conducted to quantify the through-going process and evaluate its controlling factors, including displacement pattern, cover thickness, and displacement velocity. The results indicate that simple-shear strike-slip fault zones evolve through a progressive sequence from the en échelon stage to soft-linkage, hard-linkage, and ultimately a through-going stage. Each evolutionary stage corresponds to distinct threshold values of relative displacement (D/L). En échelon faults initiate at the base of the model during the embryonic stage and propagate upward to the surface during the soft-linkage stage when D/L ranges from 1.37% to 2.38%. Subsequently, Y-shear faults link individual fault segments during the hard-linkage stage at D/L values of 2.59%–4.81%, followed by the formation of a fully through-going fault zone at D/L values of 6.14%–7.76%. Generally, displacement threshold values increase with greater cover thickness during upward fault propagation. Threshold values also increase from bilateral codirectional displacement to unilateral displacement, and further to bilateral anti-directional displacement patterns, whereas higher displacement velocities tend to reduce the threshold values. The experimentally derived quantitative evolution is consistent with the fault segmentation and linkage mechanisms observed in strike-slip faults of the central Tarim intracratonic basin. These results demonstrate that the through-going process of pure strike-slip fault zones can quantitatively constrained by displacement, while strata thickness, displacement patterns, and displacement velocity exert significant control on the corresponding threshold values.

1. Introduction

Strike-slip faults are widely distributed within the Earth's crust and exert fundamental influences on tectonic evolution, petrophysical properties, and fluid migration pathways (e.g., Sylvester, 1988; Tapponnier et al., 2001; Mann, 2007; Jourdon et al., 2026). Many fault zones display complex segmentation patterns that evolve from isolated fault segments into long through-going fault zones through progressive fault linkage and interaction (Willemse et al., 1997; Crider and Peacock, 2004; Ghosh and Chattopadhyay, 2008; Lucas et al., 2023). The growth history of strike-slip fault zones typically involves the initiation of isolated en échelon segments, followed by their interaction, propagation, linkage, and ultimately the formation of a continuous through-going fault zone. Fault-segment linkage and interaction are therefore key processes controlling the development of through-going fault zones. These processes can be influenced by multiple factors, including displacement, lithology, pre-existing structures, and inherited deformation fabrics (e.g., Aydin and Schultz, 1990; Crider and Peacock, 2004; Curren and Bird, 2014; Wu et al., 2021; Zhu et al., 2024). Case studies indicate that the through-going process often produces complex fault-zone architectures and strongly influences fluid-rock interactions.

* Corresponding author.
E-mail address: wugh@swpu.edu.cn (G.-H. Wu).
Peer review under the responsibility of China University of Petroleum (Beijing).

https://doi.org/10.1016/j.petsci.2026.05.056

In recent years, significant hydrocarbon resources have been discovered within strike-slip fault zones of the Tarim intracratonic basin in northwestern China (Ma et al., 2022; Wang et al., 2022). Many strike-slip faults in the basin are characterized by small displacements and pronounced segmentation, whereas several large-scale fault zones exhibit near through-going geometries (Yang et al., 2020; Wu et al., 2021). Fault segmentation plays a crucial role in controlling reservoir heterogeneity and hydrocarbon productivity (Ma et al., 2022; Wang et al., 2022; Yang et al., 2022; Xiong et al., 2024; Zeng et al., 2026). Although geological, geophysical, and production datasets provide valuable constraints on the through-going process of strike-slip faults, the ultra-deep (>6000 m) faults are commonly imaged by low-resolution seismic data. This limitation hampers detailed identification of fault segmentation, linkage, and interaction (Yang et al., 2020). Furthermore, strike-slip fault types, deformation mechanisms, and evolutionary histories vary significantly across different structural domains of the basin (Yang et al., 2020; Qi, 2021; Wu et al., 2021; Deng et al., 2022; Liu et al., 2023). Consequently, substantial debate remains regarding the architecture of strike-slip fault zones, their deformation styles at different evolutionary stages, and their implications for fractured reservoirs and hydrocarbon accumulation (e.g., Wang et al., 2022; Zeng et al., 2026). In this context, developing a quantitative model for the through-going evolution of strike-slip fault zones is essential for improving understanding of fault growth mechanisms and deep structural evolution.

Sandbox analogue modeling provides an effective approach for reconstructing and analyzing the evolution of complex strike-slip fault zones (Naylor et al., 1986; Dooley and Schreurs, 2012; Xiao et al., 2017; González-Muñoz et al., 2024; Zhu et al., 2024). In the Tarim Basin, analogue models have been applied to investigate en échelon fault deformation (Shi et al., 2024), conjugate strike-slip fault systems (Xiao and Tong, 2024), fault growth processes (Peng et al., 2022; Neng et al., 2025), the relationship between Riedel fracture spacing and layer thickness (Li et al., 2025), and hydrocarbon migration and accumulation (Zhu et al., 2022). These studies have provided important insights into the structural styles, formation mechanisms, and evolutionary modes of strike-slip faults. Typically, strike-slip fault zones initiate as en échelon fault arrays and progressively evolve into through-going strike-slip zones. Under pure strike-slip conditions, fault evolution has been divided into several stages, including the infancy stage, R-shear (Riedel) stage, P-shear (opposite to R-shear oblique direction) stage and Y-shear (parallel to the main displacement zone) stage, and the final through-going stages (Xiao et al., 2017). Experimental studies further demonstrate that shear strain is initially accommodated by distributed deformation, followed by the development of en échelon faults and progressive propagation toward a through-going fault zone (Hatem et al., 2017). However, quantitative constraints on the displacement thresholds associated with each evolutionary stage remain limited.

Based on the pure strike-slip tectonic setting in the central Tarim Basin, this study presents twelve sets of sandbox analogue experiments designed to quantitatively characterize the evolutionary stages of strike-slip zones and evaluate the key factors controlling the through-going process.

2. Geological background

The Tarim Basin, located in northwestern China, is a Paleo–Mesozoic intracratonic basin that has experienced multi-stage tectonic-sedimentary evolution (Jia, 1997). During the Cambrian–Early Ordovician period, an extensive carbonate platform developed across the western part of the basin (Wu et al., 2016). By the end of the Early Ordovician, subduction of the Proto-Tethys Ocean induced regional compressional deformation, resulting in the formation of east–west-trending paleo-uplifts within the basin (Fig. 1). Subsequently, the carbonate platform subsided during the Late Ordovician, and the basin evolved into a structural framework characterized by alternating north–south-oriented depressions and uplifts. Recently, a strike-slip fault-controlled petroleum system has been recognized in the central basin (Fig. 1). Strike-slip faults connect the Cambrian source rocks with the Middle–Upper Ordovician fractured carbonate reservoirs, resulting in a series of hydrocarbon accumulations distributed along strike-slip fault zones (Wang et al., 2022; Yang et al., 2022; Zhu et al., 2022; Liu et al., 2025). Consequently, fractured reservoirs of “sweet spots” associated with strike-slip fault zones have become primary drilling targets in deep Ordovician carbonates.

The Fuman oilfield, situated within the Northern Depression of the Tarim Basin, is the largest ultra-deep oilfield discovered in China (Wang et al., 2022). NE-trending strike-slip faults with lengths of approximately 50–90 km have been identified in this area (Fig. 1). These faults are mainly developed within the Cambrian–Ordovician, although some major faults extend upward into the Silurian–Devonian and Carbonate–Permian (Fig. 2; Yang et al., 2020; Deng et al., 2023). The Cambrian–Late Ordovician carbonate strata reach thickness of up to 3000 m, and are overlain by the Late Ordovician siliciclastic successions that exceed 1000 m in thickness. Integrated seismic interpretation and U–Pb dating of fracture cements indicate that the strike-slip faults initially formed during the Middle–Late Ordovician, with some major faults undergoing reactivations during the Silurian–Devonian and Carbonate–Permian periods (Yang et al., 2020; Wu et al., 2021; Liu et al., 2025).

These strike-slip faults are generally characterized by small displacements, with horizontal displacements typically less than 500 m and vertical displacements less than 80 m within the Lower Paleozoic carbonates. Displacement generally increases with fault scale and progressive growth, with higher displacement and stronger deformation commonly localized within hard-linked segments (Yang et al., 2020). Most faults exhibit clear segmentation, consisting of en échelon or oblique fault segments that represent immature fault systems transitioning from isolated to soft-linked configurations, with only a limited number of hard-linked segments (Fig. 2). In contrast, larger faults such as F_I5 and F_I17 approach fully through-going geometries and are characterized by greater displacement and length (Yang et al., 2020; Deng et al., 2022, 2023). Except for localized transpressional hard-linked zones, most segments are linear faults displaying minimal vertical deformation, consistent with a predominantly pure strike-slip regime. This structural style contrasts with the conjugate “X-type” faults in the northern uplift and transfer faults in the southern uplift (Yang et al., 2020).

The strike-slip fault system is thought to be related to the northward compression associated with closure of the Proto-Tethys Ocean (Wu et al., 2021). The pre-existing NE-trending basement structures likely facilitated the development of transfer faults in the central uplift, accommodating contraction within the NW-trending anticlinal belts (Wu et al., 2016; Yang et al., 2020). Far-field compression from south to north across the Fuman oilfield may have promoted the formation and propagation of NE-trending en échelon/oblique strike-slip fault zones (Yang et al., 2020; Wu et al., 2021; Deng et al., 2022). Progressive propagation and linkage of the isolated segments are interpreted as the primary mechanism responsible for the development of a long strike-slip fault zone with relatively small displacement (Wu et al., 2021). In addition, lithologic variations between different tectonic layers have also been proposed as an important control on

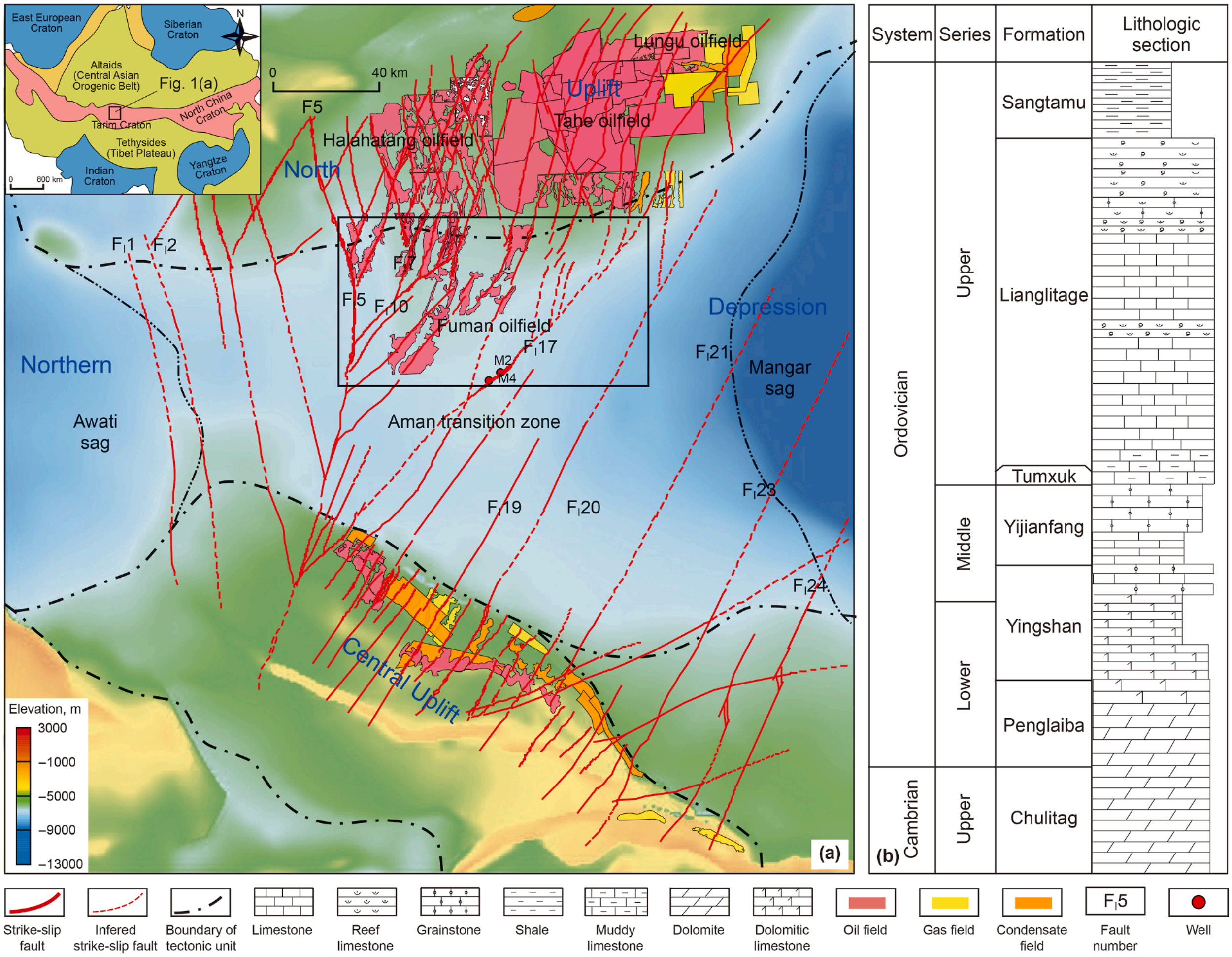

Fig. 1. **(a)** The strike-slip fault-controlled petroleum system, with the base map showing the structural outline at the top of the Ordovician carbonate, and the corner map showing the tectonic location of the Tarim Basina; **(b)** the stratigraphic column of the Cambrian–Ordovician in the central Tarim Basin (after Wang et al., 2022).

structural styles during fault evolution (Yang et al., 2020; Deng et al., 2022; Neng et al., 2025). In this context, understanding the through-going evolution of strike-slip fault zones is critical for evaluating fault segmentation, fractured reservoir distribution, and hydrocarbon accumulation within complex strike-slip fault-controlled petroleum systems (Yang et al., 2022; Wang et al., 2022).

3. Methods and data

The relatively small vertical displacement observed within strike-slip fault zones in the Fuman oilfield is consistent with a predominantly pure strike-slip regime (Yang et al., 2020; Deng et al., 2023). Accordingly, pure strike-slip analogue modeling was conducted using sandbox experiments according to geometric, kinematic, and dynamic similarity principles (Dooley and Schreurs, 2012; Xiao et al., 2017). Because the Cambrian–Ordovician carbonate succession exceeds 3000 m in thickness and exhibits relatively heterogeneous mechanical behavior, dry quartz sand was used in all experiments to simulate brittle rock deformation (Xiao et al., 2017).

The experimental kinematic setup was designed to reproduce the simple-shear strike-slip deformation inferred for the Fuman oilfield (Yang et al., 2020). Because the relative motion of the two fault walls remains uncertain, three displacement patterns were tested: (1) unilateral displacement, (2) bilateral codirectional displacement, and (3) bilateral antidirectional displacement. Since displacement patterns can significantly influence fault evolution (e.g., Schreurs, 1994; Wu et al., 2009; González-Muñoz et al., 2024), these experiments were designed to evaluate their effects on the through-going process. During each experiment, displacement (D) was measured from the onset of isolated fault segments to the development of a through-going fault zone. To enable comparison between models with different effective lengths, relative displacement (D/L; where L is the effective length) was calculated and used to characterize progressive fault evolution. This quantitative parameter provides a useful reference for seismic interpretation and evaluation of strike-slip faults in the Tarim Basin. The applied boundary conditions and driving mechanisms follow Xiao et al. (2017) and can be summarized as two main components: (1) contractional stress transmitted into the sand pack through an electric actuator and baffle system, and (2) additional contraction generated by elastic shortening of the basal rubber sheet coupled with the contractional baffle.

The model length was designed to be 700–800 mm, corresponding to natural strike-slip fault zone lengths of approximately 50–100 km (Table 1), yielding an approximate geometric scaling ratio of 1:100,000. For the quantitative stage analysis, both D and D/L were recorded for each experiment. A comparative simple-shear experiment was also conducted for validation, and structural interpretation focused primarily on surface deformation

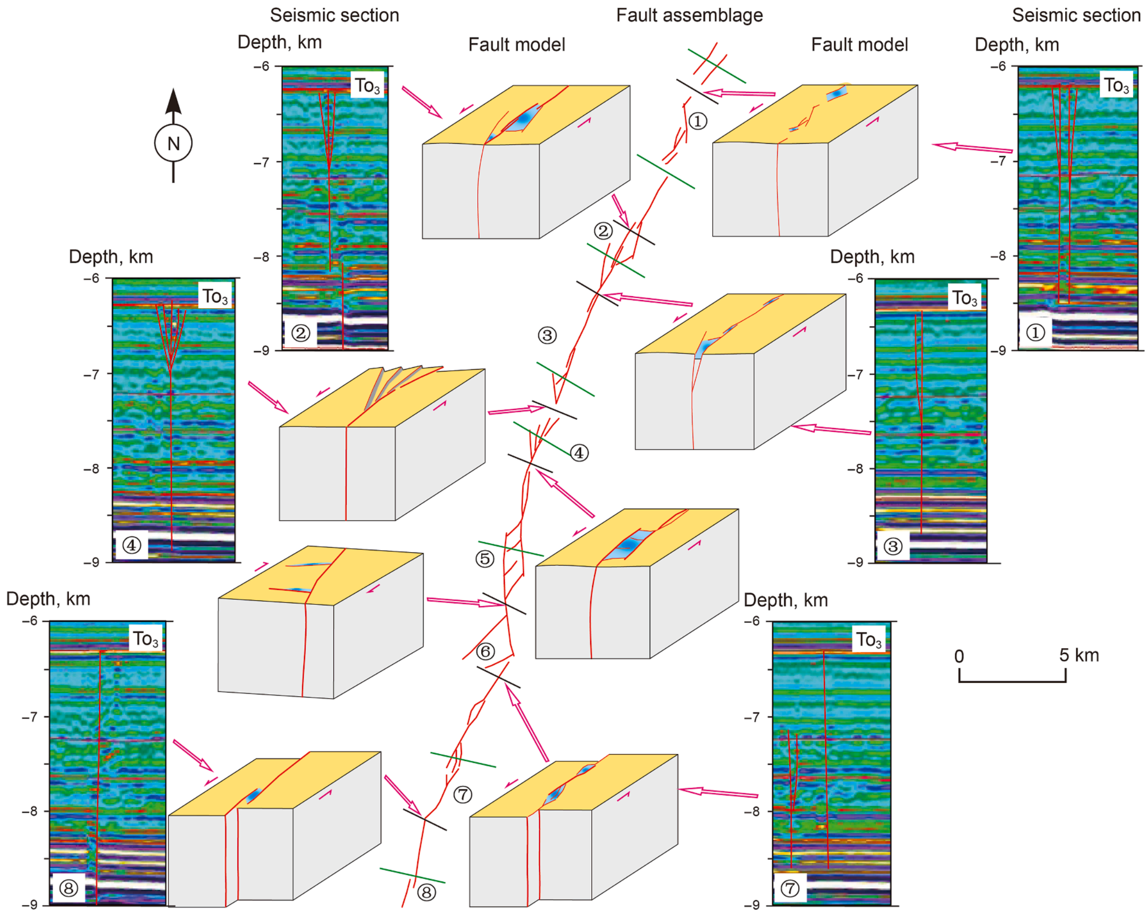

Fig. 2. The fault segment model and seismic sections of the typical strike-slip fault zone $F_{I}7$ in the Tarim Basin (red line showing strike-slip fault zone and the "bead shape" reflection showing large fracture-cave reservoir; O: overlap segment; the blue block in the model shows a falling block; To_3: base of the Upper Ordovician; see location in Fig. 1; modified after Zhu et al. (2022).

Table 1
Experimental parameters of the strike-slip fault in different evolution stages.

Experiment number	Moving type	Displacement pattern	Size, mm× mm	Thickness, mm	Velocity, mm/s	Slicing	Embryonic stage		Soft-linkage stage		Hard-linkage stage		Through-going stage	
							D, mm	*D*/*L*, %	*D*, mm	*D*/*L*, %	*D*, mm	*D*/*L*, %	*D*, mm	*D*/*L*, %
1	Right-lateral	Unilateral	500×700	50	0.02	CT	<9.6	<1.37	9.6	1.37	19.2	2.74	43	6.14
2	Right-lateral	Unilateral	500×700	50	0.01	CT	<12	<1.71	12	1.71	23	3.29	48	6.86
3	Right-lateral	Unilateral	500×700	50	0.005	CT	<11.4	<1.63	11.4	1.63	24	3.43	54	7.71
4	Right-lateral	Unilateral	500×700	80	0.005	CT	<12.8	<1.83	12.8	1.83	24.9	3.56	54.3	7.76
5	Left-lateral	Unilateral	600×800	70	0.04	No	<14.4	<1.80	14.4	1.80	30	3.75	52.8	6.60
6	Left-lateral	Bilateral codirectional	600×700	50	0.0025	CT	<13.8	<1.91	13.8	1.97	18.6	2.66	45	6.43
7	Left-lateral	Bilateral codirectional	600×700	50	0.005	Manually	<13.2	<1.89	13.2	1.89	18.1	2.59	44.1	6.30
8	Right-lateral	Bilateral antidirectional	600×800	70	0.04*0.02	No	<15.6	<1.95	15.6	1.95	31.2	3.90	56.4	7.05
9	Left-lateral	Bilateral antidirectional	600×800	70	0.04*0.02	Manually	<16	<2.00	16	2.00	33	4.13	57	7.13
10	Left-lateral	Bilateral antidirectional	600×800	70	0.04*0.005	Manually	<16.8	<2.10	16.8	2.10	35.7	4.46	58	7.25
11	Left-lateral	Bilateral antidirectional	600×800	70	0.04*0.005	Manually	<17.5	<2.19	17.5	2.19	38.5	4.81	61	7.63
12	Left-lateral	Bilateral antidirectional	600×800	100	0.075*0.005	No	<19	<2.38	19	2.38	37	4.63	60	7.50

(Size: width×length; velocity: 0.04*0.02 showing the different velocity of the two walls; the values of the late three stages are the threshold values).

patterns. Cover thickness was variable between 50 and 70 mm, corresponding to an approximate thickness scaling of ~1:50,000. This thickness ratio is larger than the length scaling because accurate observation and measurement require relatively thick sand layers (Dooley and Schreurs, 2012; Xiao et al., 2017). To evaluate the influence of cover thickness on upward fault propagation and linkage, additional experiments were conducted with a 100 mm cover thickness. Displacement velocity ranged from 0.0025 mm/s to 0.08 mm/s (Table 1). Although the implied temporal scaling differs from length scaling (reaching up to ~1:100,0000 in some cases), such velocity ranges are commonly considered appropriate in analogue modeling studies investigating rate effects on fault evolution (Dooley and Schreurs, 2012; Xiao et al., 2017).

All experiments were conducted in the Structural Simulation Laboratory at Southwest Petroleum University and the Northwest Branch of the CNPC Research Institute of Petroleum Exploration and Development. The experimental apparatus consists of a main control platform and a sandbox deformation system (Fig. 3; Xiao et al., 2017). Computed tomography (CT) scanning was used to obtain vertical and horizontal slices of selected models in order to investigate internal deformation structures. This technique relies on differences in X-ray attenuation caused by density contrasts associated with faulting (Mattioni et al., 2006; Cui et al., 2021). Four models were scanned using CT, with each scan lasting approximately 10 min. Experimental parameters and quantitative results are summarized in Table 1.

4. Experimental results

4.1. Unilateral displacement experiments

Unilateral displacement experiments (Experiments 1–5) are illustrated using Experiment 2 as a representative case (Fig. 4; Table 1).

With progressive dextral displacement in Experiment 2, multiple strike-slip-related structures developed on the model surface, including en échelon strike-slip fracture arrays (Fig. 4). At an early stage ($D = 12$ mm, $D/L = 1.71\%$), R-shear fractures initiated on the surface at an intersection angle typically greater than 15° relative to the principal displacement zone (PDZ). These fractures propagated upward from the basal discontinuity, while the fault zone remained narrow during this initiation stage, corresponding to early R-shear development. R-shear fractures tended to deflect toward the active fault wall and progressively lengthened. Overlapping segments formed soft-linked zones within stepovers.

With increasing basal displacement ($D = 23$ mm, $D/L = 3.29\%$), low-angle R-shear fractures developed together with P- and Y-shear fractures on the model surface. R-shear fractures continued to lengthen, and minor uplift associated with basal contraction locally widened the strike-slip zone. The appearance and activity of Y-shear fractures indicate the onset of hard-linkage. With further deformation ($D = 48$ mm, $D/L = 6.86\%$), abundant R-, P-, and Y-shear fractures developed, accompanied by enhanced linkage and interaction among fault segments. Subsequently, growth in fracture length and fault-zone width diminished, whereas deformation became increasingly localized within hard-linked zones where secondary fractures and damage zones interacted more intensely. Transpression produced localized uplifts, whereas transtensional segments generated small sags. Ultimately, the fracture network became connected mainly by Y-shear structures along the PDZ, marking the through-going stage. During this stage, fault-bounded horsts and sags progressively developed as fault linkage intensified. The overall fault-zone width remained nearly constant, while deformation continued to concentrate within the hard-linked zones.

Across Experiments 1–3, the displacement thresholds (D and D/L) associated with each evolutionary stage generally increased as displacement velocity decreased (Table 1). For example, when velocity decreased from 0.02 mm/s to 0.005 mm/s, the through-going threshold increased from $D = 42$ mm ($D/L = 6.00\%$) to $D = 54$ mm ($D/L = 7.71\%$). Comparisons between Experiments 3 and 4 show that increasing cover thickness also increase D and D/L thresholds for each stage. Experiment 5 simultaneously varies model length, thickness, and displacement velocity, resulting in different threshold values and suggesting that all three parameters influence the stage transitions.

4.2. Bilateral codirectional displacement experiments

Experiments 6 and 7 illustrate the bilateral codirectional displacement pattern (Fig. 5; Table 1). In Experiment 6, progressive sinistral displacement produced typical strike-slip structures on the model surface (Fig. 5). At an early stage ($D = 13.8$ mm, $D/L = 1.97\%$), R-fractures initiated within a narrow fault zone, marking the transition from the embryonic stage to the R-shear stage. Soft-linked stepovers developed as en échelon fractures propagated at their tips. With continued displacement ($D = 18.6$ mm, $D/L = 2.66\%$), low-angle R- and P-fractures appeared, while both fracture lengths and fault-zone width increased. At larger displacement ($D = 45$ mm, $D/L = 6.43\%$), R-shear fractures showed limited additional growth and the overall fault-zone width remained relatively stable. Numerous fine fractures developed within overlapped zones, and the strike-slip zone became progressively organized. Eventually, fractures connected

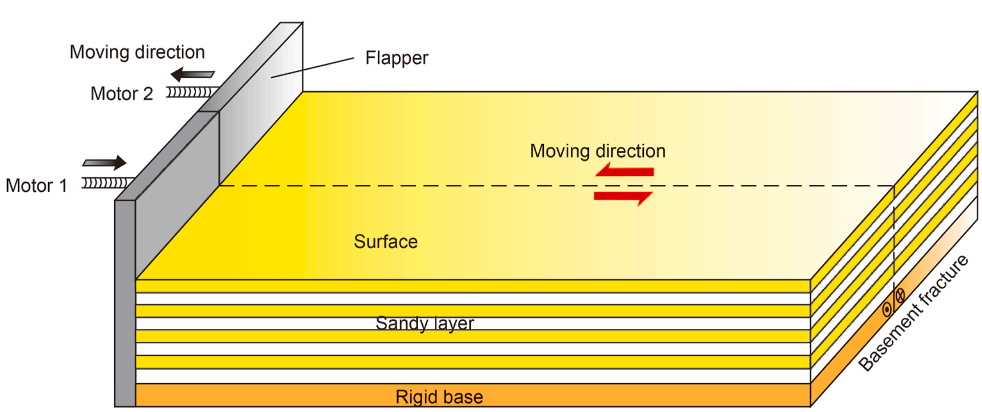

Fig. 3. Sandbox model for the through-going experiments (after Xiao et al., 2017).

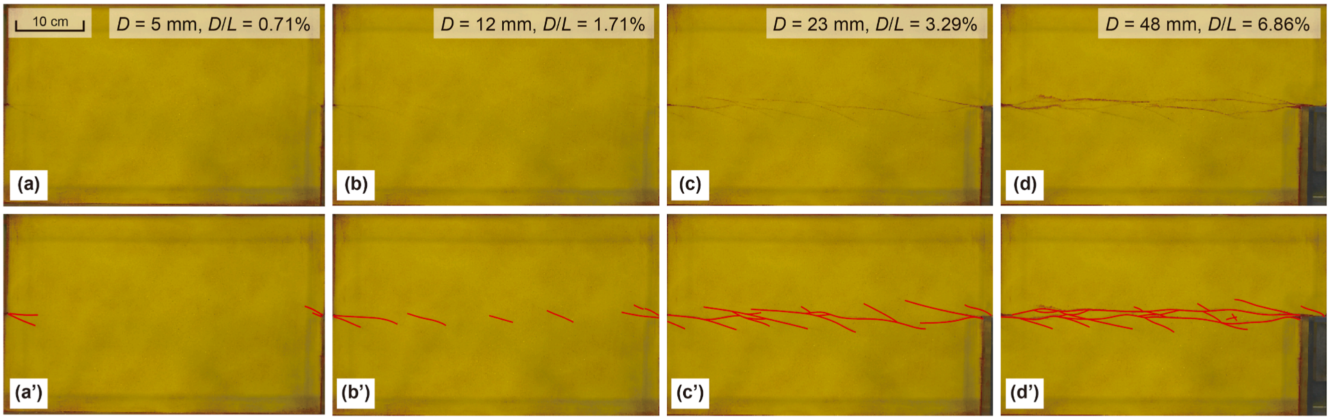

Fig. 4. The analogue models of different stages with the unilateral displacement in Experiment 2. **(a)–(d)** showing the fractures of different stages: the embryonic, soft-linkage, hard-linkage and through-going stages; **(a')–(d')** showing the interpreted images of different stages. *D*: displacement; *D*/*L*: relative displacement.

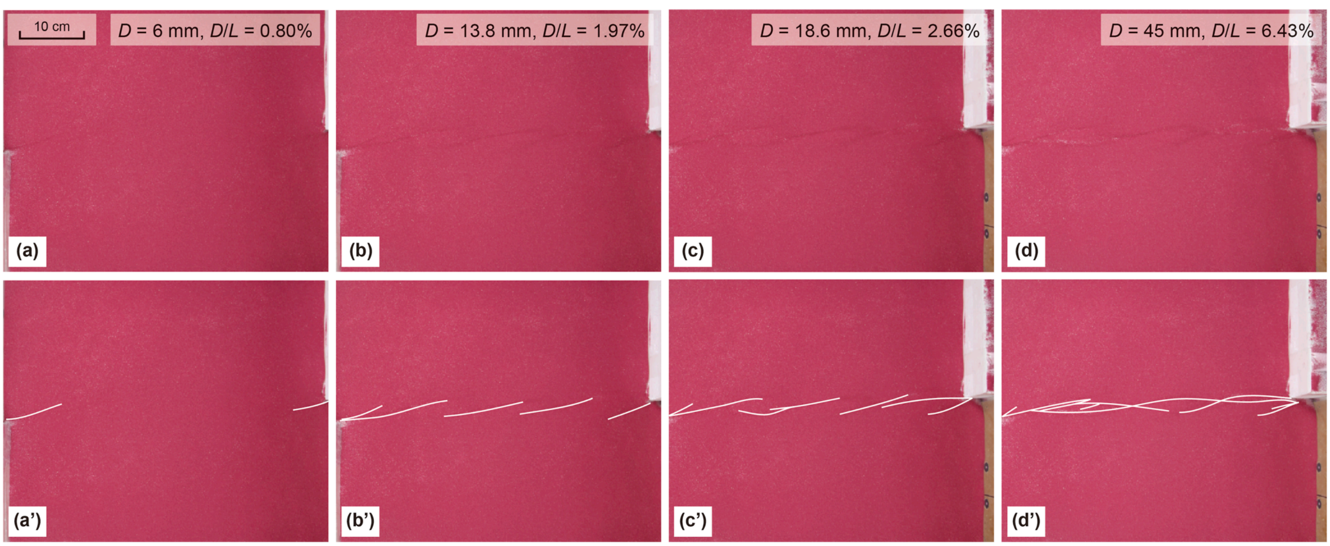

Fig. 5. The analogue models of different stages with the bilateral codirectional displacement in Experiment 6 (the subfigure labels are the same as in Fig. 4).

along the basal discontinuity direction through Y-shear fractures. Continued deformation produced persistent fracturing without additional widening of the fault zone, while Y-shear structures remained active, indicating a through-going stage.

In Experiments 6 and 7, the *D* and *D*/*L* thresholds generally decrease with increasing displacement and displacement velocity. The through-going process resembles that observed in the unilateral models. Compared with unilateral Experiments 1–4, bilateral codirectional models tend to show slightly larger *D* and *D*/*L* values during early R-shear development, but somewhat lower thresholds during Y-shear and through-going stages. This difference likely reflects the kinematic effects of bilateral motion, although variations in velocity and thickness among experiments may also contribute.

4.3. Bilateral antidirectional displacement experiments

Experiments 8–12 represent the bilateral antidirectional displacement pattern (Fig. 6; Table 1), which may better approximate the kinematics of major strike-slip faults in the Fuman oilfield (Yang et al., 2020; Deng et al., 2023). Because the relative velocity between the two fault walls equals the sum of their opposing motions, the effective shear rate in this configuration is higher than in the unilateral and codirectional models. Since some major faults in the oilfield approach through-going stage geometries, experiments in this group employed larger model length and thicker sand layers for comparison.

In Experiment 8, progressive displacement produced abundant strike-slip structures on the model surface (Fig. 6). During the early R-shear stage ($D = 15.6$ mm, $D/L = 1.95\%$), R-shear fractures appeared, and the narrow fault zone marked the transition from embryonic to R-shear development. At $D = 31.2$ mm ($D/L = 3.90\%$), low-angle R-shear fractures rapidly developed, accompanied by increases in fracture length and fault-zone width. Y-shear fractures formed and linked overlapping R-shear segments, and deformation associated with hard linkage intensified. At $D = 56.4$ mm ($D/L = 7.05\%$), R- and Y-shear lengths stabilized and fault-zone width became nearly constant, while deformation continued to intensify within hard-linked zones. At this stage, previously independent fracture sets became connected by Y- and P-shear fractures parallel to the basal discontinuity, marking the onset of the through-going stage. Continued displacement

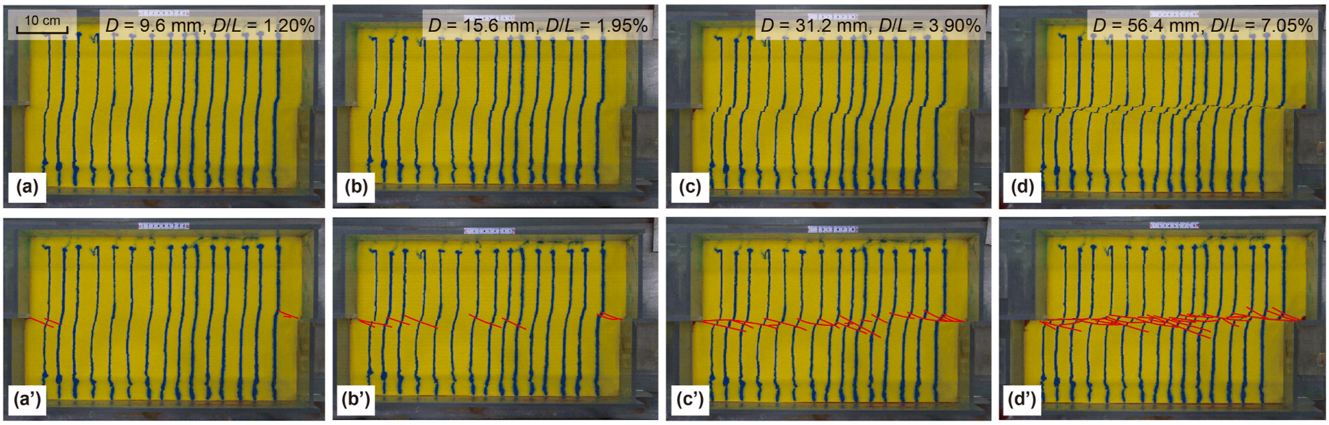

Fig. 6. The analogue models of different stages with the bilateral antidirectional displacement in Experiment 8 (the subfigure labels are same as in Fig. 4).

produced persistent internal deformation; however, the fault-zone width did not increase further, and deformation remained localized within overlap zones.

Within this experiment group, the D and D/L thresholds increase as displacement velocity decreases from Experiments 8 to 11. Consistent with the other model sets, thicker cover in Experiment 12 results in larger D and D/L thresholds. Overall, D and D/L values in the antidirectional group are generally higher than those in the other kinematic groups. However, the D/L thresholds for the through-going stage cluster within ~7.05%–7.75%, similar to those observed in unilateral Experiments 3–4.

5. Discussion

5.1. Evolutionary stages of strike-slip fault zones

Pure strike-slip fault zones are characterized by horizontal motion within an approximately isotropic mechanical environment, making them well suited for analogue modeling (Naylor et al., 1986; Schreurs, 1994; Xiao et al., 2017). The simple shear experiments presented here show broadly similar evolutionary processes for strike-slip fault zones (Table 1; Figs. 4–6). Although fracture geometries and displacement thresholds vary among models, all experiments evolve from segmented en échelon or oblique fractures toward a through-going fault zone. This evolution can be generalized into four stages: embryonic, soft-linkage, hard-linkage, and through-gonging (Fig. 7). These stages broadly correspond to the embryonic, R-shear, P-Y shear and through-going stages of Xiao et al. (2017). CT-derived 3D images further highlight the distinct internal architectures associated with these stages (Fig. 8).

During the embryonic stage, fractures propagate upward from the basal discontinuity and first appear at the model surface as en échelon/oblique segments (Figs. 4–9). In all experiments, R-shear fractures are the earliest localized structures and require finite strain to propagate from the base to the surface (Fig. 9(a)–(e)), consistent with the classic Riedel shear framework (Naylor et al., 1986; Dooley and Schreurs, 2012; Xiao et al., 2017). Because strike-slip deformation is driven by basement motion, these models highlight the importance of strain transfer from deep to shallow structural levels under pure strike-slip conditions. Horizontal CT slices further indicate vertical transmission of deformation through the cover (Fig. 8). R-shear fractures typically form en échelon or oblique arrays at the surface, which may reflect stress rotation with depth (Naylor et al., 1986; Xiao et al., 2017). Differences relative to wet kaolin experiments, in which distributed shear may precede discrete en échelon fractures, likely reflect differences in material properties and early off-fault damage (Hatem et al., 2017). Except for maximum principal stress (σ_1), off-fault fracturing may also be influenced by the magnitude and orientation of the intermediate principal stress (σ_2) (Naylor et al., 1986; Atmaoui et al., 2006; Dooley and Schreurs, 2012; Xiao et al., 2017). In our models, thickness scaling is relatively large compared with length scaling (Table 1), which may enhance the influence of σ_2. Consequently, fractures are not strictly vertical in section (Fig. 7; Xiao et al., 2017), and fault dips are less than those interpreted from Tarim seismic data (Fig. 2; Yang et al., 2020). In this context, R-shears may develop helicoidal geometries and undergo off-fault rotation, with the intersection angle between R-fracture and the PDZ decreasing with depth (Fig. 9(f)). In the central Tarim Basin, strike-slip faults within the Cambrian–Ordovician carbonates generally consist of oblique segments with small intersection angles (<15°) relative to the PDZ, whereas some en échelon segments show larger angles (Fig. 2). This depth-dependent change is commonly interpreted as reflecting multi-stage reactivation (Deng et al., 2022; Yang et al., 2020). Alternatively, progressive off-fault rotation and distributed R-shear development may also contribute to decreasing intersection angles from depth to surface.

Once en échelon or oblique fractures reach the surface, the fracture network enters the soft-linkage stage. In unilateral models, fractures tend to initiate near the driving boundary and propagate along strike (Fig. 4(a)). Segments lengthen mainly by tip propagation, forming overlap zones. However, significant interaction within overlap zones remains limited until Y-shear fractures develop and connect adjacent segments (Figs. 4–9). Segment linkage and interaction then define the hard-linkage stage, typically facilitated by Y-shear connections that promote development of a continuous deformation zone (e.g., Cartwright et al., 1995; Peacock, 2002; Kim and Sanderson, 2005; Peacock et al., 2017). During this stage, en échelon segment growth slows, and deformation becomes increasingly localized within overlap zones. P-shears are not always required for linkage in our models, which differs slightly from the combined P–Y stage described by Xiao et al. (2017). With progressive linkage, deformation concentrates along the PDZ (Fig. 7(a)). The fracture network evolves toward through-going behavior, commonly accompanied by localized horst–graben development and concentrated damage within overlap zones.

Overall, considering upward propagation from the base and progressive linkage from segmented to through-going arrays, four stages are defined for the through-going process (Fig. 7). This

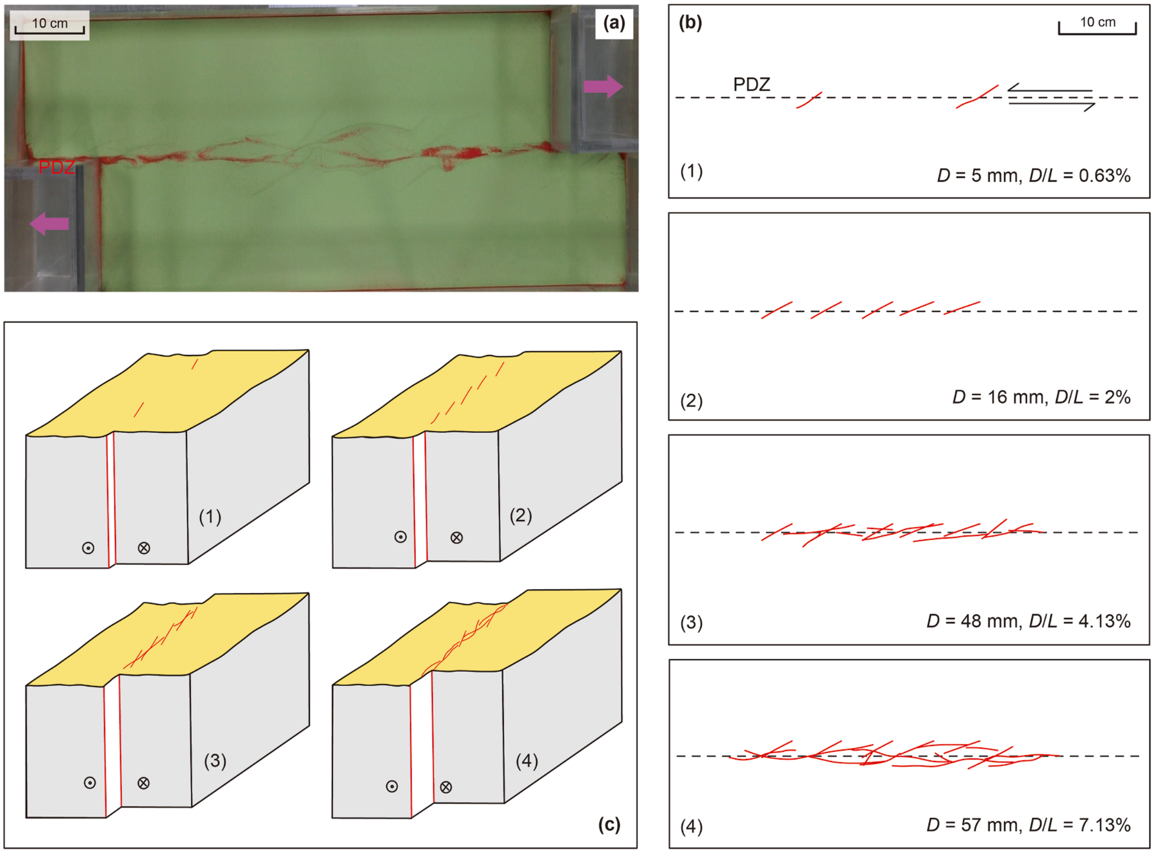

Fig. 7. **(a)** A downward sketch of the through-going stage (the curve lines show the fractures; the red blocks show the exposure of the deep layer); **(b)** the planar and **(c)** 3D sketch of the four stages showing through-going process in the pure strike-slip fault zone. (1) embryonic stage: R-shear fractures develop; (2) soft-linkage stage: R-shear fractures propagate and overlap, and the strike-slip fault zone width is relatively narrow; (3) hard-linkage stage: Y-shear fractures develop and link, and the width of strike-slip faults increases and en échelon fractures are hard-linked and interact; (4) through-going stage: Y-shear fractures link to be a through-going fault zone, and the unified displacement occurs along the main fault zone.

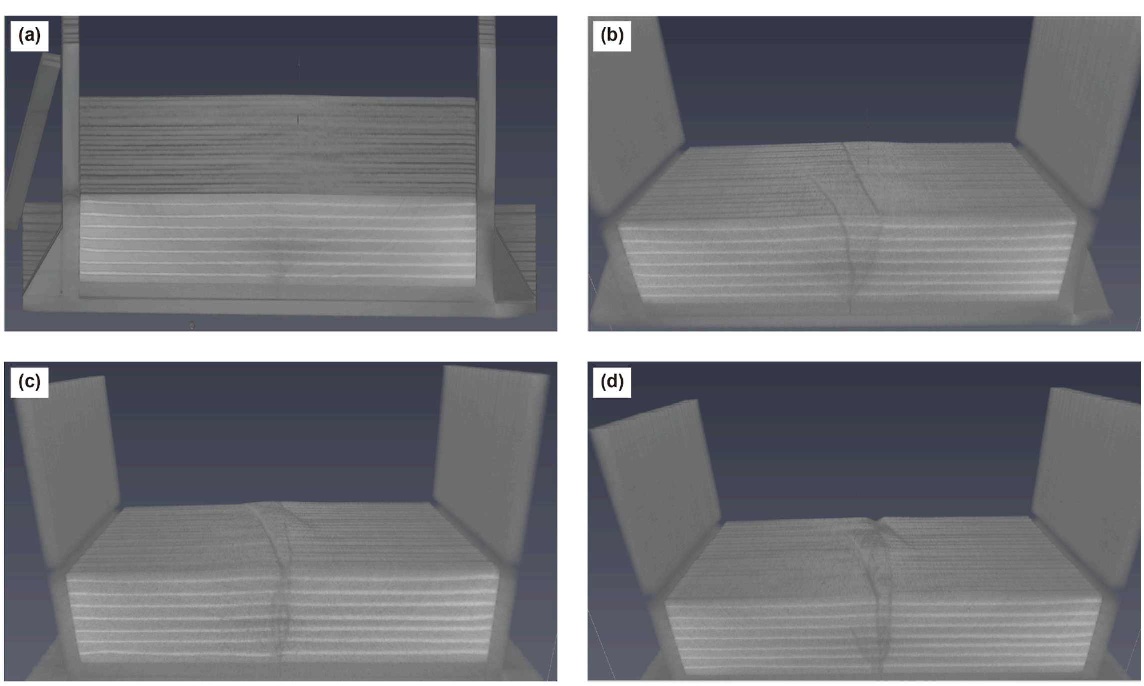

Fig. 8. 3D modeling by CT images for the four-stage evolution of the strike-slip zone: **(a)** the embryonic, **(b)** soft-linkage, **(c)** hard-linkage and (d) through-going stages. The black lines show the fractures.

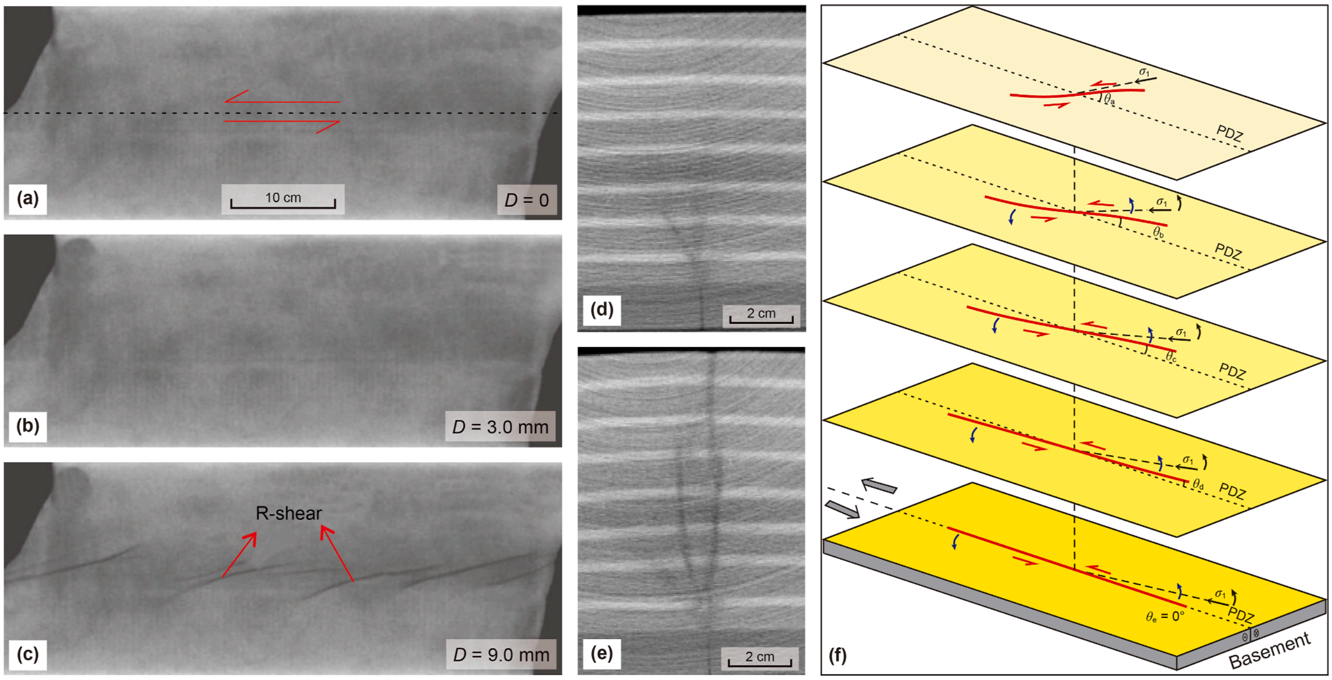

Fig. 9. The deformation and fractures at the surface of the sandbox with displacement **(a–c)**, and the sections by CT photos **(d, e)** in Experiment 8; **(f)** sketch model of the R-shear fracture growth from base to cover surface (modified after Xiao et al., 2017). θ: intersection angle between the fault and PDZ.

framework is broadly consistent with previous analogue studies (Naylor et al., 1986; Schreurs, 1994; Dooley and Schreurs, 2012; Xiao et al., 2017; González-Muñoz et al., 2024), although different materials and deformation mechanisms may produce distributed strain or alternative fracture networks during the earliest stage (Hatem et al., 2017). The linkage-driven through-going process is also widely documented in natural strike-slip systems (Sylvester, 1988; Willemse et al., 1997; Kim and Sanderson, 2005; Torabi and Berg, 2011; Pennacchioni and Mancktelow, 2013; Bramham et al., 2021; Kumar et al., 2023; Liu et al., 2023; Abdelhaleem et al., 2024). In the Tarim Basin, many immature strike-slip faults present evolutionary sequences from isolated to soft-linked, hard-linked, and locally through-going structures (Wu et al., 2020, 2021; Yang et al., 2020; Liu et al., 2023). Unlike the predominantly Y-shear linkage observed in our experiments, segment propagation and interaction may play a stronger role in the Tarim Ordovician reservoirs because many segments intersect the PDZ at relatively low angles (Fig. 2). This mechanism differs from models invoking sequential vertical linkage between lower and upper fault levels (Deng et al., 2019). Therefore, oblique segment propagation and interaction may be particularly important for through-going development in the Ordovician carbonate rocks of the Tarim Basin.

5.2. *Quantification of the through-going process of strike-slip fault zones*

Strike-slip fault zones generally comprise multiple segments that progressively link to form a through-going fault zone (e.g., Kelly et al., 1998; Swanson, 2006). Analogue studies have documented this linkage process from isolated segments to through-going structures (Rahe et al., 1998; Dooley and Schreurs, 2012; Xiao et al., 2017), and natural examples from the Tarim intracratonic basin further highlight the importance of segmentation and linkage during fault-zone growth (Wu et al., 2020; Liu et al., 2023). In our experiments, the soft- and hard-linkage stages are particularly diagnostic for evaluating the through-going process (Figs. 4–9), because fracture types and displacement thresholds vary systematically with progressive linkage and can therefore be quantified.

Both displacement (D) and relative displacement (D/L) show consistent relationships with the identified evolutionary stages (Figs. 10 and 11), supporting their use for quantitative stage definition. Given the strong correlation between D and D/L (Fig. 10) and the variability in absolute displacement among natural cases, D/L provides a more robust metric for quantifying the through-going process. The boundary between the embryonic stage and the onset of R-shear development is defined by the first appearance of R-shear fractures at the model surface. When D/L is less than 1.37%–2.38% (Fig. 11, Table 1), R-shear fractures initiate during the embryonic stage and form scattered en échelon or oblique fractures intersecting the PDZ at angles typically less than 20°. These embryonic fractures remain isolated and do not develop significant overlap zones, consistent with the small displacement

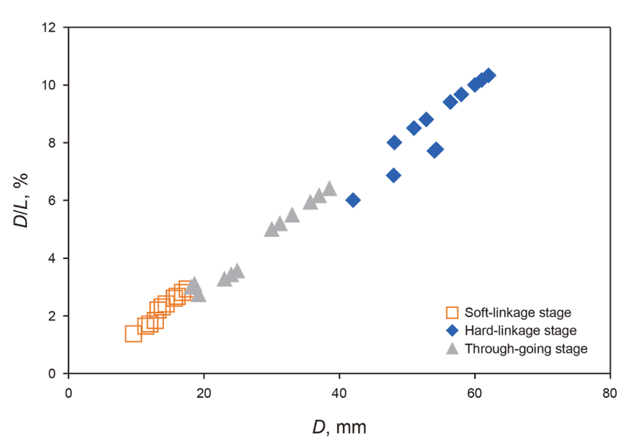

Fig. 10. The D–D/L correlation of the analogue models at different stages.

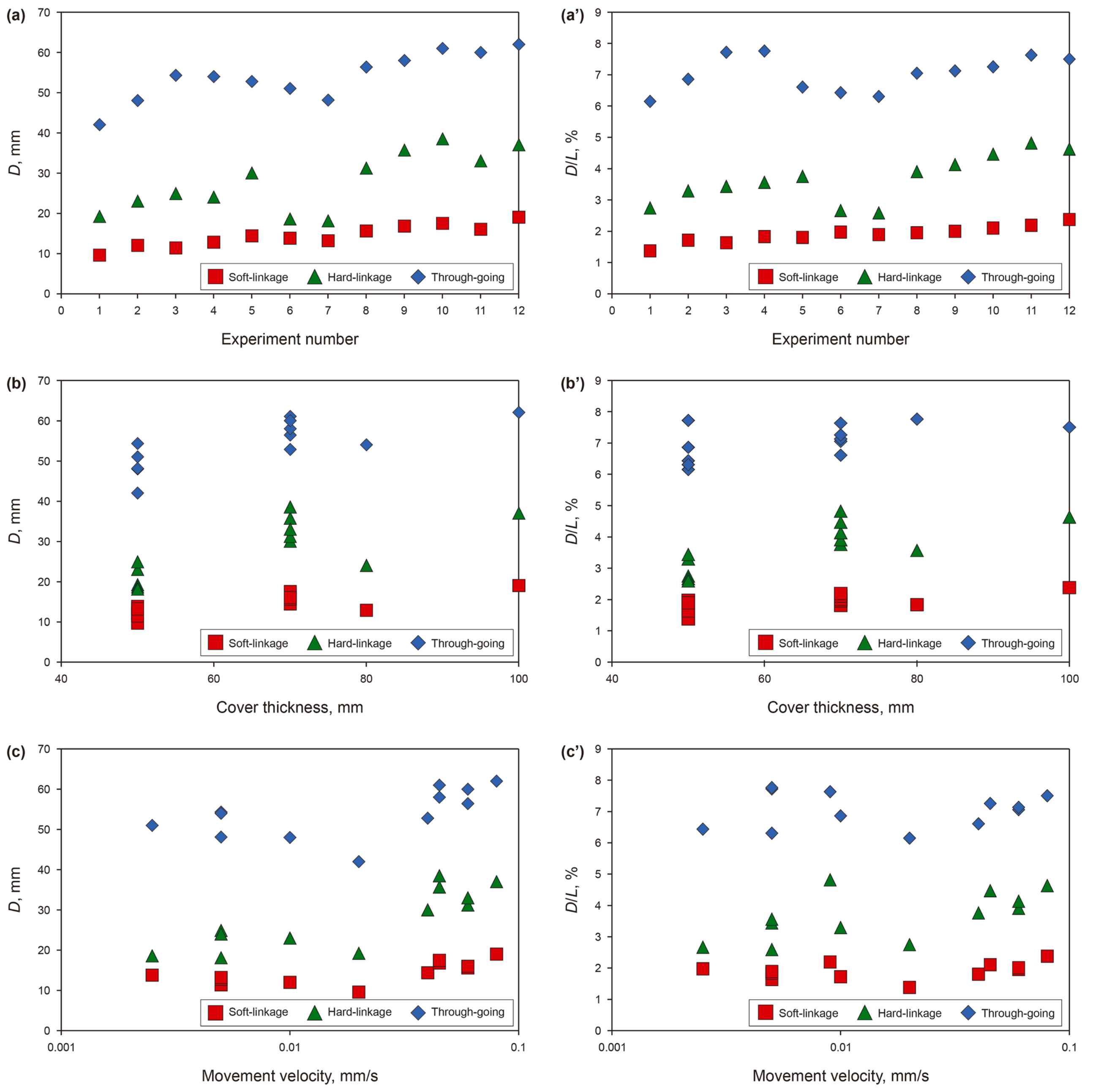

Fig. 11. The *D* and *D*/*L* values vary in different stages with the different displacement patterns **(a)**, cover thickness **(b)** and displacement velocity **(c)**. The data are from Table 1.

associated with early strike-slip evolution (Xiao et al., 2017) (see Fig. 12).

With increasing displacement, the number and length of R-shear fractures increase (Figs. 4–6, 8), and en échelon or oblique segments progressively approach one another, generating soft-linkage within overlap zones. R-shear fractures continue to lengthen by tip propagation, although growth rates commonly decrease and splay fractures may develop near segment tips. A decreased intersection angle between R-shears and the PDZ may further promote overlap and linkage. Minor P- and Y-shear fractures may also initiate during this interval. When *D*/*L* increases to approximately 2.59%–4.81% (Fig. 11; Table 1), soft-linkage becomes predominant along strike, although localized hard-linkage may occur where Y-shears connect adjacent R-shears. At this stage, segmentation remains pronounced, consistent with analogue and natural examples of immature strike-slip fault zones (Dooley and Schreurs, 2012; Barcos et al., 2016; Xiao et al., 2017; Yang et al., 2020).

As displacement continues to accumulate, Y-shear fractures increasingly connect R-shear segments, producing hard-linkage between fracture networks (Figs. 4–6, 8). Parallel en échelon fractures interact through Y-shear connections, strengthening secondary fracturing and localized deformation within overlap zones. Localized faulted horsts and grabens develop within these zones, reflecting segment interaction and linkage-related strain localization (Xiao et al., 2017). Although such linkage and interaction are readily recognized in analogue experiments, they are difficult to resolve in the ultra-deep subsurface of the Tarim Basin using conventional seismic imaging (Wu et al., 2016, 2020). In natural cases, the presence of Y-shear connections and along-strike structural relief may serve as indirect indicators of segment interaction and hard-linkage, potentially reflected by

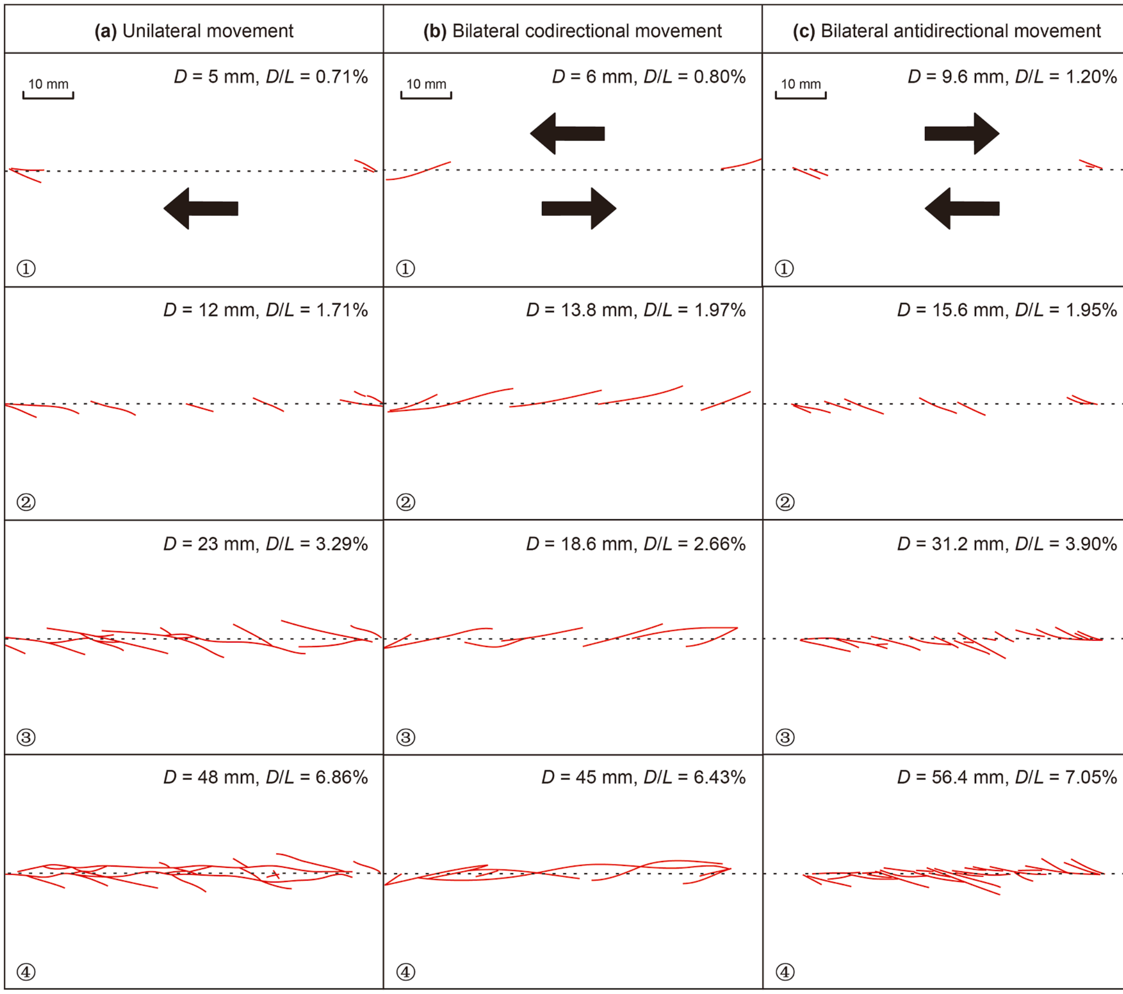

Fig. 12. The fracture network comparison between unilateral **(a)**, bilateral codirectional **(b)**, and bilateral antidirectional **(c)** displacement experiments. ①: embryonic stage; ②: soft-linkage stage; ③: hard-linkage stage; ④: through-going stage; the black arrow showing the movement direction.

localized fractured rocks and enhanced deformation within overlap zones (Fig. 2).

When D/L exceeds approximately 6.14%–7.76% (Fig. 11; Table 1), the fault zone enters the through-going stage, characterized by a connected deformation corridor along the PDZ. In analogue models, the through-going geometry is readily identified (Figs. 4–6, 8), whereas in the deep Tarim Basin it can remain ambiguous. Because vertical displacement at segment tips is generally limited under pure strike-slip conditions, along-strike variations in vertical displacement or structural relief may provide a useful proxy for identifying through-going behavior in seismic interpretation. At this stage, increased basal displacement produces distinct stratigraphic offset and a continuous PDZ, while internal fractures become increasingly interconnected and deformation becomes concentrated along the PDZ. The fault zone approaches a more mature through-going architecture in which deformation and displacement become more laterally continuous, in contrast to the strongly segmented displacement distribution of earlier stages. This evolution differs from strike-slip systems in continental margins, where through-going faults commonly develop larger displacements and different scaling relationships (e.g., Sylvester, 1988; Woodcock and Schubert, 1994; Curren and Bird, 2014). In the Tarim intracratonic basin, most strike-slip fault zones likely remain in immature soft- to hard-linkage stages and have not yet reached a fully through-going stage (Yang et al., 2020). Some studies suggest that initial fractures may form near the top or bottom of the cover and be followed by new fractures developing within intermediate layers (Neng et al., 2025), which warrants further analogue and theoretical investigation.

Repeatability is supported by experiments conducted under comparable conditions (e.g., Experiments 3–4 and 8–9), which yield similar D and D/L thresholds with deviations typically less than 1% (Table 1). Nevertheless, some variability remains (Table 1; Fig. 11), likely reflecting sensitivity to basal configuration, sand preparation, and boundary conditions. Unilateral experiments show larger scatter among stage thresholds, suggesting greater sensitivity to asymmetric boundary motion and operational effects. Thicker sand packs, slower displacement rates, and more tightly controlled experimental preparation may reduce this scatter. In addition, the D and D/L values cluster more tightly at the through-going stage than during earlier transitional stages. Higher-resolution displacement monitoring and slower displacement rates may further improve constraints on threshold values for different stages.

Overall, the relative displacement (D/L) metric effectively captures the progressive through-going process in simple-shear strike-slip fault zones and provides quantitative thresholds for the transitions through R-shear development, soft-linkage, hard-linkage, and the through-going stage.

5.3. Factors influencing the through-going process

Previous studies indicate that strike-slip fault formation and architecture can be influenced by regional and local stress fields, kinematic pattern, pre-existing structures, and rock mechanical properties (Naylor et al., 1986; Aydin and Schultz, 1990; Richard et al., 1995; Crider and Peacock, 2004; Ma et al., 2009; Curren and Bird, 2014; Barcos et al., 2016). Analogue experiments commonly show progressive evolution from isolated segments to through-going fault zones (Dooley and Schreurs, 2012; Barcos et al., 2016; Xiao et al., 2017). Our experiments also reveal stage-dependent ranges in displacement thresholds under pure strike-slip conditions, implying that multiple factors modulate the through-going process. Therefore, we focus on the roles of displacement pattern, cover thickness, and displacement velocity within the quantitative framework established above.

5.3.1. Displacement pattern

Displacement pattern exerts a first-order control on the through-going process (Table 1; Fig. 11(a) and (a'), 12). In general, stage thresholds (D and D/L) increase from bilateral codirectional to unilateral and then to bilateral antidirectional models. Codirectional motion may facilitate upward propagation of deformation from the basal discontinuity into the cover, which is broadly consistent with codirectional strike-slip kinematics inferred for parts of the central uplift in the Tarim Basin (Wu et al., 2016; Yang et al., 2020). Differences in velocity between the two fault walls may also promote propagation of transfer faults from the base to the shallow subsurface, potentially contributing to the higher degree of connectivity reported in some structural domains. However, the relationship between pure strike-slip faults and transfer faults requires further investigation.

Within our pure strike-slip experiments, antidirectional models show more stable D/L thresholds than unilateral models. For example, D/L values at the through-going stage vary by approximately 9% in antidirectional models but by approximately 21% in unilateral models, and variability in earlier stages can exceed 30% in unilateral experiments. This suggests that unilateral experiments are more susceptible to boundary-condition sensitivity and operational effects, potentially because unilateral driving requires the active wall to transmit motion to the passive wall, introducing greater mechanical and experimental instability.

5.3.2. Cover thickness

The cover thickness can influence both R-shear length and the width of the strike-slip fault zones (Atmaoui et al., 2006; Xiao et al., 2017). In our experiments, D/L generally increases with increasing cover thickness (Fig. 11(b), (b')), indicating that thick cover delays the attainment of through-going connectivity and requires larger relative displacement thresholds. This trend suggests that cover thickness is an important control on the displacement required to reach the through-going stage. Correlations appear weaker during the soft- and hard-linkage stages, implying that early-stage fracture growth may be less sensitive to thickness than the final development of a continuous PDZ. This difference suggests that deformation mechanisms may differ between early segment-growth stages and later through-going development.

In the Tarim Basin, fault-zone width and en échelon spacing or width have been linked to the overburden thickness (Deng et al., 2019), supporting the importance of stratigraphic thickness. However, layered deformation in natural examples is often overprinted by multiple deformation phases (Deng et al., 2019; Yang et al., 2020), complicating direct comparison. Because thickness scaling in our models exceeds length scaling (Table 1), the experiments produce relatively smaller fault dips and complex internal geometries. Further work is therefore needed to isolate the subtle effects of thickness, stratigraphic heterogeneity, and basement structural inheritance.

5.3.3. Displacement velocity

Displacement velocity also influences the through-going process (Fig. 11(c), (c'); Table 1). Except for the single fastest experiment, unilateral and bilateral antidirectional models show a general decrease in D and D/L thresholds with increasing velocity, suggesting that shear rate can modulate fracture initiation and linkage (Dooley and Schreurs, 2012; Hatem et al., 2017; Xiao et al., 2017). However, in experiments with thicker covers (e.g., Experiments 5 and 12), the highest velocities appear less sensitive, implying that thickness-related effects may partly mask the influence of velocity.

In the Tarim intracratonic basin, strike-slip displacement rates are likely slower than in many continental-margin strike-slip fault systems (Sylvester, 1988; Yang et al., 2020), which may contribute to the requirement for larger cumulative displacement to achieve through-going connectivity. Because natural displacement rates remain poorly constrained, additional case studies are needed to better evaluate rate effects.

5.4. Implications for subsurface strike-slip fault patterns and evolution

Case studies indicate that en échelon/oblique segments are widespread at different depths and displacement levels prior to through-going development of strike-slip fault zones in the Tarim Basin (Yang et al., 2020). Given that the relative displacement (D/L) of major strike-slip fault zones in the Tarim Basin is commonly less than 6% (Yang et al., 2020; Wu et al., 2021; Deng et al., 2022), most fault zones are unlikely to have entered the fully through-going stage, consistent with analogue-based strike-slip fault evolution models in this study. This highlights the need for detailed segmentation-focused interpretation of intracratonic strike-slip fault systems in the deep subsurface.

Seismic attribute enhancement often produces apparently continuous strike-slip fault traces in the Tarim intracratonic basin (Yang et al., 2020; Wang et al., 2022). On seismic sections, small-scale strike-slip faults may appear as a single steep fault plane (Fig. 2). However, measured displacements of strike-slip faults in the Tarim Basin are generally small (D/L < 5%) (Wu et al., 2016, 2020; Yang et al., 2020; Deng et al., 2022), and most major strike-slip faults show horizontal offsets of less than 500 m. The largest offset estimated from the Cambrian platform markers reaches approximately 670 m (Du et al., 2020). In some large fault zones, apparent horizontal displacement ranges from 300 m to 770 m and may reach approximately 1817 m based on offsets measured from seismic horizontal slices (Deng et al., 2019), while values up to 1780 m have been reported in the central uplift (Han et al., 2017). These apparent displacements may be influenced by the geometry of transfer faults, the distance between fault walls, and stratigraphic or structural deviations in seismic slicing (Yang et al., 2020). The broad displacement range likely reflects both measurement uncertainty and genuine segmentation-related variability, consistent with our experimental results.

Our analogue results suggest that fault zones with small displacement are generally too immature to be fully through-going, supporting interpretations of pronounced segmentation in both fault architecture and reservoir compartmentalization (Wu et al., 2020; Wang et al., 2022; Yang et al., 2022). Seismic attribute patterns and fault styles of large strike-slip faults also indicate along-strike segmentation (Yang et al., 2020). Even where some segments appear hard-linked, a small-displacement fault zone does not necessarily constitute a fully through-going structure, consistent with the D/L-based stage thresholds established in this study. In the central Tarim Basin, small-scale strike-slip faults commonly comprise en échelon or oblique segments (Deng et al., 2022, 2023), matching the patterns in our experiments. As en échelon faults merge downward into the PDZ and accommodate strike-slip displacement, transtensional en échelon faults above the Ordovician should not necessarily be interpreted as normal faults (Han et al., 2017; Deng et al., 2019).

Intracratonic strike-slip fault zones with small displacement typically contain multiple soft- and hard-linked segments (e.g. Yang et al., 2020). Segment linkage can produce substantial fault-length growth, commonly greater than 50 km, potentially doubling fault-zone length without a proportional increase in displacement and thereby deviating from power-law displacement–length scaling relationships (Torabi and Berg, 2011; Ma et al., 2019; Wu et al., 2020, 2021). In such systems, secondary fault splays commonly align with the maximum principal stress direction, while deformation and displacement concentrate within overlap zones between segments. Unlike mature through-going faults, this segmented linkage style produces localized strain concentration in hard-linked stepovers (Kim and Sanderson, 2005; Faulkner et al., 2010; Wu et al., 2020), leading to long fault zones with relatively small displacement. This behavior has important implications for hydrocarbon migration, trapping, and reservoir compartmentalization in the Tarim Basin (Wu et al., 2016, 2021; Deng et al., 2022; Yang et al., 2022; Liu et al., 2023). Reservoirs and fluids may be compartmentalized by fault segmentation, forming a series of segment-controlled hydrocarbon accumulations along the strike-slip corridors.

In many natural cases, quantifying the through-going process remains challenging because it is influenced by lithology, rock properties, preexisting structures, and faulting mechanisms (Sylvester, 1988; Crider and Peacock, 2004; Curren and Bird, 2014; Bramham et al., 2021; Kumar et al., 2023; Abdelhaleem et al., 2024). Nevertheless, many strike-slip systems undergo progressive linkage from isolated segments to through-going fault zones (Cartwright et al., 1995; Peacock, 2002; Kim and Sanderson, 2005; Torabi and Berg, 2011; Durand-Riard et al., 2013; Peacock et al., 2017; Lucas et al., 2023). Their geometric and kinematic characteristics can therefore be related to specific evolutionary stages. Although displacement thresholds may vary over a wide range owing to different controlling factors, the D/L-based quantitative framework proposed here provides a practical tool for stage discrimination and subsurface interpretation, particularly for small-displacement intracratonic strike-slip systems such as those in the Tarim Basin.

6. Conclusions

This study provides the following key conclusions regarding the through-going process of pure strike-slip fault zones.

(1) Under pure strike-slip conditions, fault zones evolve through four progressive stages—embryonic, soft-linkage, hard-linkage, and through-going—driven by segment propagation, interaction, and linkage.
(2) The stage transitions of a strike-slip fault zone can be quantitatively constrained by relative displacement (D/L), with threshold ranges of 1.37%–2.38%, 2.59%–4.81%, and 6.14%–7.76% corresponding to the successive transitions to surface R-shear development, linkage-dominated growth, and through-going connectivity, respectively.
(3) Displacement thresholds for different stages increase with increasing cover thickness and generally increase from bilateral codirectional to unilateral and then to bilateral antidirectional displacement patterns, whereas higher displacement velocity tends to reduce threshold values.
(4) The quantitative analogue framework developed here provides a useful reference for discriminating segmentation and linkage mechanisms in strike-slip fault zones and supports improved interpretation of intracratonic strike-slip systems in the deep subsurface.

CRediT authorship contribution statement

Guang-Hui Wu: Writing – review & editing, Conceptualization, Investigation. **Chen Qiu:** Visualization, Validation, Software, Investigation. **Hao Tang:** Visualization, Software. **Zhou Xie:** Supervision, Resources. **Xin Chen:** Data curation, Investigation.**Heng-You Li:** Validation, Resources. **Zhe-Yu Luo:** Data curation. **Chong Sun:** Resources.

Declaration of interests

The authors declare that they have no known competing financial interests or personal relationships that could have appeared to influence the work reported in this paper.

Acknowledgements

We thank Tao Zhang, Yang Xiao, Yu-Ting Song, Shuai Yang, Bing-Shan Ma and Xing-Xing Zhao for their assistance with the experiments and data collection. We also appreciate the reviewers and editors for constructive comments that substantially improved the manuscript. This study was partly supported by the National Natural Science Foundation of China (U24B2019, 42402163), Natural Science Foundation of Sichuan Province (2024NSFSC0814).

References

Abdelhaleem, S., Taylor, W.J., Reid, A., et al., 2024. Geometry, kinematics, and mechanics of the interaction between strike-slip and normal faults in active rifts: An example from the Quaternary-active Kane Springs Wash fault zone, Nevada, USA. Geosphere 20 (2), 290–314. https://doi.org/10.1130/ges02646.1.
Atmaoui, N., Kukowski, N., Stöckhert, B., et al., 2006. Initiation and development of pull-apart basins with Riedel shear mechanism: Insights from scaled clay experiments. Int. J. Earth Sci. 95 (2), 225–238. https://doi.org/10.1007/s00531-005-0030-1.
Aydin, A., Schultz, R.A., 1990. Effect of mechanical interaction on the development of strike-slip faults with echelon patterns. J. Struct. Geol. 12 (1), 123–129. https://doi.org/10.1016/0191-8141(90)90053-2.
Barcos, L., Díaz-Azpiroz, M., Balanyá, J.C., et al., 2016. Analogue modelling of inclined, brittle–ductile transpression: Testing analytical models through natural shear zones (external betics). Tectonophysics 682, 169–185. https://doi.org/10.1016/j.tecto.2016.05.021.
Bramham, E.K., Wright, T.J., Paton, D.A., et al., 2021. A new model for the growth of normal faults developed above pre-existing structures. Geology 49 (5), 587–591. https://doi.org/10.1130/G48290.1.
Cartwright, J.A., Trudgill, B.D., Mansfield, C.S., 1995. Fault growth by segment linkage: An explanation for scatter in maximum displacement and trace length data from the Canyonlands Grabens of SE Utah. J. Struct. Geol. 17 (9), 1319–1326. https://doi.org/10.1016/0191-8141(95)00033-A.
Crider, J.G., Peacock, D.C.P., 2004. Initiation of brittle faults in the upper crust: A review of field observations. J. Struct. Geol. 26 (4), 691–707. https://doi.org/10.1016/J.JSG.2003.07.007.
Cui, J., Jia, D., Wang, H.B., et al., 2021. A method to simulate the migration and accumulation of hydrocarbon with analogue modeling. Geofluids 2021, 6660760. https://doi.org/10.1155/2021/6660760.
Curren, I.S., Bird, P., 2014. Formation and suppression of strike-slip fault systems. Pure Appl. Geophys. 171 (11), 2899–2918. https://doi.org/10.1007/s00024-014-0826-7.
Deng, S., Li, H.L., Zhang, Z.P., et al., 2019. Structural characterization of intracratonic strike-slip faults in the central Tarim Basin. AAPG Bull. 103 (1), 109–137. https://doi.org/10.1306/06071817354.
Deng, S., Zhao, R., Kong, Q.F., et al., 2022. Two distinct strike-slip fault networks in the Shunbei area and its surroundings, Tarim Basin: Hydrocarbon accumulation, distribution, and controlling factors. AAPG Bull. 106 (1), 77–102. https://doi.org/10.1306/07202119113.

Deng, X.L., Chen, J.J., Cao, P., et al., 2023. Segmentation and lateral growth of intracratonic strike-slip faults in the northern Tarim Basin, NW China: Influences on Ordovician fault-controlled carbonate reservoirs. Front. Earth Sci. 11, 1255162. https://doi.org/10.3389/feart.2023.1255162.

Dooley, T.P., Schreurs, G., 2012. Analogue modelling of intraplate strike-slip tectonics: A review and new experimental results. Tectonophysics 574–575, 1–71. https://doi.org/10.1016/j.tecto.2012.05.030.

Du, J., Ma, D.B., Liu, W., et al., 2020. Structural characteristics and formation mechanism of faults in Xiaotangnan area, Tarim Basin, NW China. Nat. Gas Geosci. 31 (5), 658–666. https://doi.org/10.11764/j.issn.1672-1926.2020.04.015 (in Chinese).

Durand-Riard, P., Shaw, J.H., Plesch, A., et al., 2013. Enabling 3D geomechanical restoration of strike- and oblique-slip faults using geological constraints, with applications to the deep-water Niger Delta. J. Struct. Geol. 48 (3), 33–44. https://doi.org/10.1016/j.jsg.2012.12.009.

Faulkner, D.R., Jackson, C.A.L., Lunn, R.J., et al., 2010. A review of recent developments concerning the structure, mechanics and fluid flow properties of fault zones. J. Struct. Geol. 32 (11), 1557–1575. https://doi.org/10.1016/j.jsg.2010.06.009.

Ghosh, N., Chattopadhyay, A., 2008. The initiation and linkage of surface fractures above a buried strike-slip fault: An experimental approach. J. Earth Syst. Sci. 117 (1), 23–32. https://doi.org/10.1007/s12040-008-0009-y.

González-Muñoz, S., Schreurs, G., Schmid, T.C., et al., 2024. Influence of lateral heterogeneities on strike-slip fault behaviour: Insights from analogue models. Solid Earth 15 (12), 1509–1523. https://doi.org/10.5194/se-15-1509-2024.

Han, X.Y., Deng, S., Tang, L.J., et al., 2017. Geometry, kinematics and displacement characteristics of strike-slip faults in the northern slope of Tazhong uplift in Tarim Basin: A study based on 3D seismic data. Mar. Petrol. Geol. 88, 410–427. https://doi.org/10.1016/j.marpetgeo.2017.08.033.

Hatem, A.E., Cooke, M.L., Toeneboehn, K., 2017. Strain localization and evolving kinematic efficiency of initiating strike-slip faults within wet kaolin experiments. J. Struct. Geol. 101 (8), 96–108. https://doi.org/10.1016/j.jsg.2017.06.011.

Jia, C.Z., 1997. Structure Features and Petroleum in Tarim Basin of China. Petroleum Industry Press, Beijing (in Chinese).

Jourdon, A., Le Pourhiet, L., May, D.A., et al., 2026. Lithospheric models supported by the Caribbean and Levant examples help rethink transpression at plate boundaries. Nat. Commun. 17, 1290. https://doi.org/10.1038/s41467-025-68051-2.

Kelly, P.G., Sanderson, D.J., Peacock, D.C.P., 1998. Linkage and evolution of conjugate strike-slip fault zones in limestones of Somerset and Northumbria. J. Struct. Geol. 20 (11), 1477–1493. https://doi.org/10.1016/S0191-8141(98)00048-0.

Kim, Y.S., Sanderson, D.J., 2005. The relationship between displacement and length of faults: A review. Earth Sci. Rev. 68 (3–4), 317–334. https://doi.org/10.1016/j.earscirev.2004.06.003.

Kumar, P.C., Sain, K., Omosanya, K.O.L., 2023. Geometry and kinematics of strike-slip faults in the Dibrugarh field of the Upper Assam foreland basin, NE India. Mar. Petrol. Geol. 153, 106291. https://doi.org/10.1016/j.marpetgeo.2023.106291.

Li, C.S., Li, S.J., Hu, Z.Q., et al., 2025. Growth mechanisms of small-displacement strike-slip faults in cratonic basins: Insights from material point method simulations. Processes 13 (6), 1946. https://doi.org/10.3390/pr13061946.

Liu, Y., Suppe, J., Cao, Y.C., et al., 2023. Linkage and formation of strike-slip faults in deep basins and the implications for petroleum accumulation: A case study from the Shunbei area of the Tarim Basin, China. AAPG Bull. 107 (2), 331–355. https://doi.org/10.1306/11142220110.

Liu, Z., Tian, J.Q., Hao, F., et al., 2025. Differential (re-)activation and hydrocarbon enrichment of segments of intracratonic strike-slip faults in the central Tarim Basin, northwestern China. AAPG Bull. 109 (10), 1233–1257. https://doi.org/10.1306/05072524042.

Lucas, L.C.V., Vasconcelos, D.L., Balsamo, F., et al., 2023. Interaction and linkage of basin-boundary fault segments control deformation bands distribution and damage zone permeability. J. Struct. Geol. 176, 104958. https://doi.org/10.1016/j.jsg.2023.104958.

Ma, B.J., Qi, J.F., Niu, S.Y., et al., 2009. The influence of basement fault on the deformation of complex cover blocks in a uniform stress field: Enlightenment from sandbox experiment. Earth Sci. Front. 16 (4), 105–116. https://doi.org/10.3321/j.issn:1005-2321.2009.04.011 (in Chinese).

Ma, D.B., Wu, G.H., Scarselli, N., et al., 2019. Seismic damage zone and width–throw scaling along the strike-slip faults in the Ordovician carbonates in the Tarim Basin. Pet. Sci. 16 (4), 752–762. https://doi.org/10.1007/s12182-019-0352-4.

Ma, Y.S., Cai, X.Y., Yun, L., et al., 2022. Practice and theoretical and technical progress in exploration and development of Shunbei ultra-deep carbonate oil and gas field, Tarim Basin, NW China. Petrol. Explor. Dev. 49 (1), 1–20. https://doi.org/10.1016/S1876-3804(22)60001-6.

Mann, P., 2007. Global catalogue, classification and tectonic origins of restraining- and releasing bends on active and ancient strike-slip fault systems. Geol. Soc. Lond. Spec. Publ. 290 (1), 13–142. https://doi.org/10.1144/SP290.2.

Mattioni, L., Le Pourhiet, L., Moretti, I., 2006. Rifting through a heterogeneous crust: Insights from analogue models and application to the Gulf of Corinth. Geol. Soc. Lond. Spec. Publ. 253 (1), 213–231. https://doi.org/10.1144/GSL.SP.2006.253.01.11.

Naylor, M.A., Mandl, G., Supesteijn, C.H.K., 1986. Fault geometries in basement-induced wrench faulting under different initial stress states. J. Struct. Geol. 8 (7), 737–752. https://doi.org/10.1016/0191-8141(86)90022-2.

Neng, Y., Xie, Z., Shao, L.F., et al., 2025. Structural physical simulation experiment on vertical growth process of strike-slip faults in ultra-deep strata of Tarim Basin,NW China. Petrol. Explor. Dev. 52 (5), 1179–1192. https://doi.org/10.1016/S1876-3804(25)60634-3.

Peacock, D.C.P., 2002. Propagation, interaction and linkage in normal fault systems. Earth Sci. Rev. 58 (1–2), 121–142. https://doi.org/10.1016/S0012-8252(01)00085-X.

Peacock, D.C.P., Nixon, C.W., Rotevatn, A., et al., 2017. Interacting faults. J. Struct. Geol. 97 (4), 1–22. https://doi.org/10.1016/j.jsg.2017.02.008.

Peng, Z.J., Feng, L., Luo, C.M., et al., 2022. Physical simulation experiment on stratification strike-slip fault deformation mechanism in the Tazhong Uplift. Geoscience 36, 1022–1034. https://doi.org/10.19657/j.geoscience.1000-8527.2022.203 (in Chinese).

Pennacchioni, G., Mancktelow, N.S., 2013. Initiation and growth of strike-slip faults within intact metagranitoid (neves area, eastern Alps, Italy). Geol. Soc. Am. Bull. 125 (9–10), 1468–1483. https://doi.org/10.1130/B30832.1.

Qi, L.X., 2021. Structural characteristics and storage control function of the Shun I fault zone in the Shunbei region, Tarim Basin. J. Petrol. Sci. Eng. 203, 108653. https://doi.org/10.1016/j.petrol.2021.108653.

Rahe, B., Ferrill, D.A., Morris, A.P., 1998. Physical analog modeling of pull-apart basin evolution. Tectonophysics 285 (1–2), 21–40. https://doi.org/10.1016/S0040-1951(97)00193-5.

Richard, P.D., Naylor, M.A., Koopman, A., 1995. Experimental models of strike-slip tectonics. Pet. Geosci. 1 (1), 71–80. https://doi.org/10.1144/petgeo.1.1.71.

Schreurs, G., 1994. Experiments on strike-slip faulting and block rotation. Geology 22 (6), 567–570. https://doi.org/10.1130/0091-7613(1994)022<0567:EOSSFA>2.3.CO;2.

Shi, S.Y., Ding, W.L., Han, J., et al., 2024. Deformation characteristics and genesis of the no. 12 strike-slip fault in the Shunbei area, Tarim Basin: Insights from 3D seismic data and physical simulation. Carbonates Evaporites 39 (4), 102. https://doi.org/10.1007/s13146-024-01020-w.

Swanson, M.T., 2006. Late Paleozoic strike-slip faults and related vein arrays of Cape Elizabeth, Maine. J. Struct. Geol. 28 (3), 456–473. https://doi.org/10.1016/j.jsg.2005.12.009.

Sylvester, A.G., 1988. Strike-slip faults. Geol. Soc. Am. Bull. 100 (11), 1666–1703. https://doi.org/10.1130/0016-7606(1988)100<1666:SSF>2.3.CO;2.

Tapponnier, P., Xu, Z.Q., Roger, F., et al., 2001. Oblique stepwise rise and growth of the Tibet Plateau. Science 294 (5547), 1671–1677. https://doi.org/10.1126/science.105978.

Torabi, A., Berg, S.S., 2011. Scaling of fault attributes: A review. Mar. Petrol. Geol. 28 (8), 1444–1460. https://doi.org/10.1016/j.marpetgeo.2011.04.003.

Wang, Q.H., Zhang, Y.T., Xie, Z., et al., 2022. The advancement and challenges of seismic techniques for ultra-deep carbonate reservoir exploitation in the Tarim Basin of northwestern China. Energies 15 (20), 7653. https://doi.org/10.3390/en15207653.

Willemse, E.J.M., Peacock, D.C.P., Aydin, A., 1997. Nucleation and growth of strike-slip faults in limestones from Somerset. U.K. J. Struct. Geol. 19 (12), 1461–1477. https://doi.org/10.1016/S0191-8141(97)00056-4.

Woodcock, N.H., Schubert, V., 1994. Continental strike-slip tectonics. In: Hancock, P.L. (Ed.), Continental Deformation. Pergamon Press, New York, pp. 251–263.

Wu, G., Kim, Y.S., Su, Z., et al., 2020. Segment interaction and linkage evolution in a conjugate strike-slip fault system from the Tarim Basin, NW China. Mar. Petrol. Geol. 112, 104054. https://doi.org/10.1016/j.marpetgeo.2019.104054.

Wu, G., Ma, B., Han, J., et al., 2021. Origin and growth mechanisms of strike-slip faults in the central Tarim cratonic basin, NW China. Petrol. Explor. Dev. 48 (3), 595–607. https://doi.org/10.1016/S1876-3804(21)60048-4.

Wu, J.E., McClay, K., Whitehouse, P., et al., 2009. 4D analogue modelling of transtensional pull-apart basins. Mar. Petrol. Geol. 26 (8), 1608–1623. https://doi.org/10.1016/j.marpetgeo.2008.06.007.

Xiao, K.Z., Tong, H.M., 2024. Analogue modelling of conjugate strike-slip faults. Front. Earth Sci. 12, 1493537. https://doi.org/10.3389/feart.2024.1493537.

Xiao, Y., Wu, G., Lei, Y., et al., 2017. Analogue modeling of through-going process and development pattern of strike-slip fault zone. Petrol. Explor. Dev. 44 (3), 368–376. https://doi.org/10.1016/S1876-3804(17)30043-5.

Xiong, C., Cai, Z.X., Ma, B.S., et al., 2024. Controls of strike-slip faults on condensate gas accumulation and enrichment in the Ordovician carbonate reservoirs of the central Tarim Basin, NW China. J. Asian Earth Sci. 263, 106019. https://doi.org/10.1016/j.jseaes.2024.106019.

Yang, H.J., Wu, G.H., Han, J.F., et al., 2020. Structural analysis of strike-slip faults in the Tarim intracratonic basin. Chin. J. Geol. 55 (1), 1–16. https://doi.org/10.12017/dzkx.2020.001 (in Chinese).

Yang, X.W., Han, J.F., Wu, G.H., et al., 2022. Controls of strike-slip Faults on Reservoir Formation and Hydrocarbon Enrichment in the Tarim Basin. Petroleum Industry Press, Beijing (in Chinese).

Zeng, L.B., Yao, Y.T., Song, Y.C., et al., 2026. Differential deformation of small- to medium-scale strike-slip faults and its control on carbonate fracture–cavity reservoir and hydrocarbon accumulation in the ultra-deep Tarim Basin. Earth Sci. Rev. 276, 105443. https://doi.org/10.1016/j.earscirev.2026.105443.

Zhu, M.J., Wang, G.Z., Li, S.Z., et al., 2024. An overview of structures associated with bends of strike-slip faults: Focus on analogue and numerical models. Mar. Petrol. Geol. 167, 106983. https://doi.org/10.1016/j.marpetgeo.2024.106983.

Zhu, Y.F., Zhang, Y.T., Zhao, X.X., et al., 2022. The fault effects on the oil migration in the ultra-deep Fuman Oilfield of the Tarim Basin, NW China. Energies 15 (16), 5789. https://doi.org/10.3390/en15165789.

Wu, G., Pang, X., Li, Q., et al., 2016. The Structural Characteristics of Carbonate Rocks and Their Effects on Hydrocarbon Exploration in Craton Basin: A Case Study of the Tarim Basin. Science Press, Beijing (in Chinese).